Russian Geology and Geophysics © 2019, V.S. Sobolev IGM, Siberian Branch of the RAS
Vol. 60, No. 2, pp. 193–203, 2019 *DOI:10.15372/RGG2019015* *Geologiya i Geofizika*

Laboratory Investigations into the Velocities and Attenuation of Ultrasonic Waves in Sand Samples Containing Water/Ice and Methane and Tetrahydrofuran Hydrates

A.D. Duchkov [a, ✉], G.A. Dugarov [a], A.A. Duchkov [a,b], A.A. Drobchik [a]

[a] *A.A. Trofimuk Institute of Petroleum Russian Geology and Geophysics, Siberian Branch of the Russian Academy of Sciences, pr. Akademika Koptyuga 3, Novosibirsk, 630090, Russia*

[b] *Novosibirsk State University, ul. Pirogova 2, Novosibirsk, 630090, Russia*

Received 23 November 2017; received in revised form 16 April 2018; accepted 15 June 2018

Abstract—The paper considers the results of a series of laboratory experiments (more than 100) on the formation of synthetic sand samples containing water/ice and methane or tetrahydrofuran hydrates in the pore space and of the measurement of their acoustic properties (velocities and attenuation of acoustic waves). The main aim of the experiments was to establish the relationship between the velocities of acoustic waves and the ice or hydrate saturation of the samples. An increase in the content of ice and hydrates always leads to a velocity increase. However, the rate of the velocity increase is determined by the localization of ice and hydrates in the samples: at the contacts between the sand grains ("cementing" model) or in the pore space ("filling" model). It has been established that the "cementing" model, characterized by a drastic initial increase in velocities, works for ice or gas hydrates formed from free methane and localized in the pores. On the contrary, tetrahydrofuran hydrates form by the "filling" model and cause a slow increase in velocities.

Keywords: water/ice-containing sand samples, methane and tetrahydrofuran hydrates, laboratory measurements, acoustic properties, velocities and attenuation

INTRODUCTION

The stable interest to both natural and technogenic gas hydrates that has been growing in the last decades is explained by their fuel value; possible effect on the environment related to greenhouse gas emission hydrates produce during decomposition; and by possibility of the technogenic disasters caused by formation or decomposition of hydrates (Istomin and Yakushev, 1992; Sloan, 2003; Makogon et al., 2007). Today most deposits of methane hydrates have been discovered in the upper layer (300–500 m in thickness) of nonconsolidated bottom sediments of marginal seas and Lake Baikal (Mazurenko and Soloviev, 2003). A number of countries (USA and Canada since 2005, Japan since 2013, China since 2017) have been carrying industrial-scale experiments aimed at the production of gas from these deposits. In Russia methane hydrate accumulation have been discovered in the bottom sediments of the Black Sea, Caspian Sea, Sea of Okhotsk and in freshwater Lake Baikal (Ginzburg and Soloviev, 1994; Khlystov, 2006; Obzhirov et al., 2012). The issue of studying hydrates in Russia remains especially actual due to growing interest to studying and development of the Arctic region that has all the necessary condition for accumulation of gas hydrates both on land and in the sediments of the northern seas.

Prospecting for gas hydrate deposits in offshore bottom sediments heavily relies on geophysical methods, whose efficiency is determined by the correlation between the sediments' physical properties and hydrate saturation (Akselrod, 2009; Waite et al., 2009; Gabito and Tsouris, 2010; Riedel et al., 2010; Ye and Liu, 2013). Knowing the physical properties (acoustic, electromagnetic, thermal, and mechanic) of hydrate-bearing sediments is crucially important not only for proper calibration of distant geophysical methods but also for undersetuping of the nature and the physical and chemical conditions of gas hydrate accumulation as well as for development and effective application of gas hydrate deposit development methods. Today hydrates are most actively studied in the USA, Japan, China, and Germany.

What attracts scientists' main attention is the acoustic properties of gas hydrates (*P*- and *S*-wave velocities and their attenuation), since seismic studies and acoustic logging have been the first-hand tools used in prospecting and studying of gas-hydrate deposits since the discovery of BSR (Bottom Simulating Reflectors) in marine seismic profiles in the 1970s (Ginsburg and Soloviev, 1994). BSR presence is an important indicator of possible gas hydrate presence in a sedimentary section.

The acoustic properties of hydrate-bearing sediments are determined by many factors such as the sediments' mineral composition and structure and the hydrate's concentration and positioning in pores. The plurality of these factors as

✉ Corresponding author.
E-mail adress: DuchkovAD@ipgg.sbras.ru (A.D. Duchkov)

well as of sedimentary rocks and the absence of a reference database that connects seismic parameters and hydrate concentration leads to a necessity to increase the amounts of experimental data, especially when new objects are under study. There have been a lot of publications covering the subject, but the issue still preserves its topicality, especially taking into account the recently completed American project into measurement and interpretation of seismic wave velocities and their attenuation in hydrate-bearing sediments whose cost has exceeded 850 thousand USD (Measurement…, 2017).

While teams of foreign scientists mainly concentrate on studying the physical properties of highly-mineralized marine sediments, Russian scientists contribute their attention in the first place to limnetic or weakly-mineralized sediments of Lake Baikal, northern seas and the cryolithozone, containing ice and hydrates. To study the acoustic properties of these rocks, in 2014–2015 a team of scientists from the Institute of Petroleum Geology and Geophysics and the Institute of Inorganic Chemistry of the Siberian Branch of the Russian Academy of Sciences developed and assembled a first-in-Russia laboratory setup to model hydrate-bearing samples and measure their acoustic properties. More details about the setup, its methods of application and first results can be found in (Duchkov et al., 2015, 2017a, b, 2018; Dugarov et al., 2017; Manakov and Duchkov, 2017). The biggest series of experiments (more than 100) was performed in 2016. The presented paper discusses the obtained results.

EQUIPMENT, SAMPLE PREPARATION TECHNIQUES, AND MEASUREMENT METHODS

The laboratory setup is a high-pressure cylinder-shaped chamber (inner diameter of 30 mm and height of 40–50 mm) with the performance range up to 45 MPa combined with a number of systems that support pressure (P) and temperature (T) maintaining and changing, injecting fluid and gas into a sample, measuring a sample length and the velocities of compressional (v_P) and shear (v_S) waves. For acoustic wave excitation and registration piezoceramic sensors with the performance frequency range of 300–700 kHz and the theoretical capacity of 1.8 W are used. To place nonconsolidated samples in the chamber one uses special measurement cells (external diameter of 30 mm and internal—of 26.6 mm) made of Caprolon or Teflon with grids or caps closing their ends. The cells are composed of two compatible parts and can change their height along the axis providing good acoustic contact with a sample during its compaction. To imitate all-around compression and prevent its deformation, a cell is compressed radially by a rubber seal (Duchkov et al., 2015).

All the described experiments were performed using specially prepared (synthetic) samples, whose known composition make them convenient for studying the correlation between acoustic parameters and pore content of ice and hydrate. These measurements in synthetic samples have become the basis of the multiple semiempirical relations, effective velocity and hydrate—concentration models for sediments (Dvorkin and Nur, 1996; Lee et al., 1996; Ecker et al., 1998; Dvorkin et al., 1999, 2000; Riedel et al., 2010; Hu et al., 2010) that are necessary for estimation of hydrate saturation from seismic data. In our experiments, the samples were formed from quartz sand mixed with distilled water and hydrate former. The sand had been selected because multiple studies of natural gas-hydrate accumulations had confirmed sand sediments to be the most perspective (Riedel et al., 2010). As hydrate former, we used methane (CH_4) and a water solution of tetrahydrofuran (THF, C_4H_8O). In nature, THF hydrate does not exist, but its chemical properties are close to methane hydrate, which forms relatively easily from THF water solution at atmospheric pressure and low positive temperature (around 1–4 °C) (Knunyants, 1983). For that reason, THF is often used instead of gas for laboratory modeling of hydrate-bearing rocks (Lee et al., 2007; Waite et al., 2009). The downside of THF is that it is a volatile matter and a good dissolver, so cells made of Teflon had to be used.

In the series of experiments, three groups of sand samples were studied with their pores filled with water/ice or methane hydrate or THF. Each experiment included three sequential operations: (i) preparation of samples with different fluid concentration (distilled water or THF water solution); estimation of the samples' porosity (Kp ~ 0.3–0.4), density and other initial characteristics; (ii) applying corresponding pressure and temperature, so either ice or hydrate are formed in the samples; (iii) acoustic signals and other parameters (P, T, sample height) were measured every 3–5 min throughout the experiment.

The setup allows to perform experiments in the conditions close to triaxial compression. The axial and lateral pressure were provided by pneumatic accumulators at the level of 25–28 MPa that made it possible to obtain high-quality acoustic signals and a relatively high pore pressure (12–13 MPa) when working with methane hydrates. The samples' temperature varied from 15 to –15°C, in most cases in cycles. The cycles (freezing/defreezing cycles) were implemented to intensify hydrate formation (when working with methane) (Chuvilin and Gur'eva, 2009; Li et al., 2011), to test the operation stability of the automation system, and to identify possible sample property changes in case of long-term experiments.

Since a common duration of an experiment was a few days (up to 10), a special attention was paid to automation of the acoustic measurements and data collecting. The designed automation system started up the setup, regulated experiment parameters according to the settings, preprocessed and visualized acoustic data and other experimental parameters (P, T, sample length) in real time. Each test started from measuring the reference samples made of Plexiglas or aluminum.

The main set of output data included P- and S-wave sets measured every 3–5 min, comprising thousands of trace

pairs for each experiment. The arrival times were calculated from the first trace extremum, which reduced the velocities by about 4%. The acoustic parameters were calculated automatically. These data were used to estimate *P*- and *S*-wave velocities relative to an estimated sample length (GOST, 1975). The calculated velocities were used to compute such elastic parameters as Poisson's ratio and Young's modulus (YM).

The tests performed using the reference samples (Plexiglas and aluminum) showed that under conditions providing a clear acoustic signal, the relative measurement error of ultrasound-wave v_P and v_S did not exceed 1%. In nonconsolidated samples, the relative measurement accuracy for acoustic velocities was about 5–6% due to the effect of the different factors related to sample formation and ensuring a contact between the sample and sensors.

Acoustic spectra analysis and attenuation value calculations were performed in a semiautomatic mode. Here it should be noted that the attenuation value of elastic oscillations can be estimated based on different parameters such as an attenuation factor, a logarithmic attenuation decrement and an inverse Q-factor (Q^{-1}). For the purposes of this study the inverse Q-factor values were calculated using the spectral ratio method (Tonn, 1991):

$$Q^{-1} = \mathrm{k}/(\pi \cdot \mathrm{t}), \quad (1)$$

where *t*, denotes the signal transit time in seconds; *k*, the inclination angle of the linear interpolation of a logarithm for a ratio between the amplitude spectra of the waves having passed through a studied sample and a reference sample with high Q-factor (namely, aluminum) in seconds. So, the attenuation values given and analyzed further in this paper are inverse Q-factor values.

EXPERIMENTAL RESULTS

The main objective of the experiments was verifying the relationship between the acoustic properties (velocity and attenuation) of the synthetic samples imitating nonconsolidated sediments, and their water/ice/hydrate volumetric content. The experience gained earlier by foreign researchers (Dvorkin et al., 2000; Waite et al., 2009; Riedel et al., 2010; Ye and Liu, 2013) demonstrates that increase of hydrate (and ice) concentration in a sample always results in faster velocities of elastic wave propagation in hydrate-bearing samples, while the character (rate) of this growth is determined by the structure of hydrate placing in the pore space (Fig. 1). In this respect, we considered two main models of hydrate (ice) saturation, which are "filling" (Fig. 1*a*, *b*) and "cementing" ones (Fig. 1*c*, *d*) ones.

In the presence of the filling saturation pattern, hydrate is formed in a sample's pore space but does not cement it at the first stage. In this case, *P*- and *S*-wave velocities grow gradually together with hydrate forming in pores. On the other hand, in case of cementing pattern, acoustic wave velocities start increasing abruptly even at low hydrate concentrations. The cementing pattern manifests itself in two ways: as "contact" (Fig. 1*c*) and "envelope" cementing (Fig. 1*d*) (Dvorkin et al., 2000). All the models listed are extreme examples of hydrate (ice) saturation of pore space, and during experiments, some transitional cases were observed. However, for interpretation of the results obtained only these four patterns were considered.

Acoustic measurements in ice-saturated samples. Frozen rock is widespread in Russia and it may contain not only ice but also gas hydrates (Yakushev, 2009). For that reason, we were interested in comparing the acoustic properties of rocks saturated with ice or hydrates. To do so, we first studied the acoustic properties of sand samples, and the way these properties changed upon initial water saturation (S_w). While preparing the samples different amounts of water were added into the sand to obtain different water-saturation values: from $S_w = 0$ (dry samples) to $S_w = 0.95$ (almost all the pores are taken with water, and at negative temperature—with ice). The S_w values, as well as the samples' density and porosity, were estimated while preparing the samples. As an example, in Fig. 2 you can see the results of one of the experiments with a sample, whose pores are almost totally filled with water ($S_w = 0.92$). The experiment lasted 15 h.

During 15 h, the sample underwent 4 freezing/defreezing cycles with *T* varying from 11 to –12 °C. The water-ice phase transitions can be well traced from the abrupt velocity

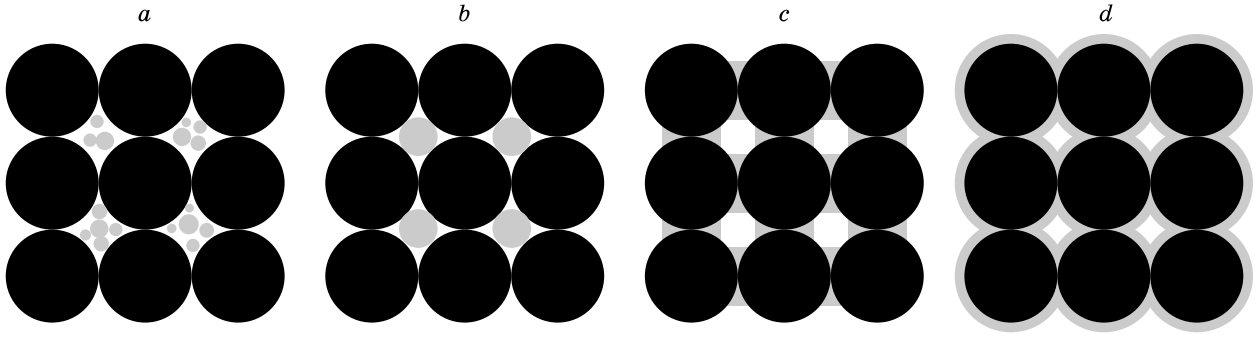

Fig. 1. Different models of gas hydrate distribution in rocks. *a*, Pore-filling; *b*, load-bearing; *c*, contact cementing; *d*, envelope cementing (Ecker et al., 1998; Dvorkin et al., 2000). Gray color marks hydrates, black—mineral particles, white—pore space.

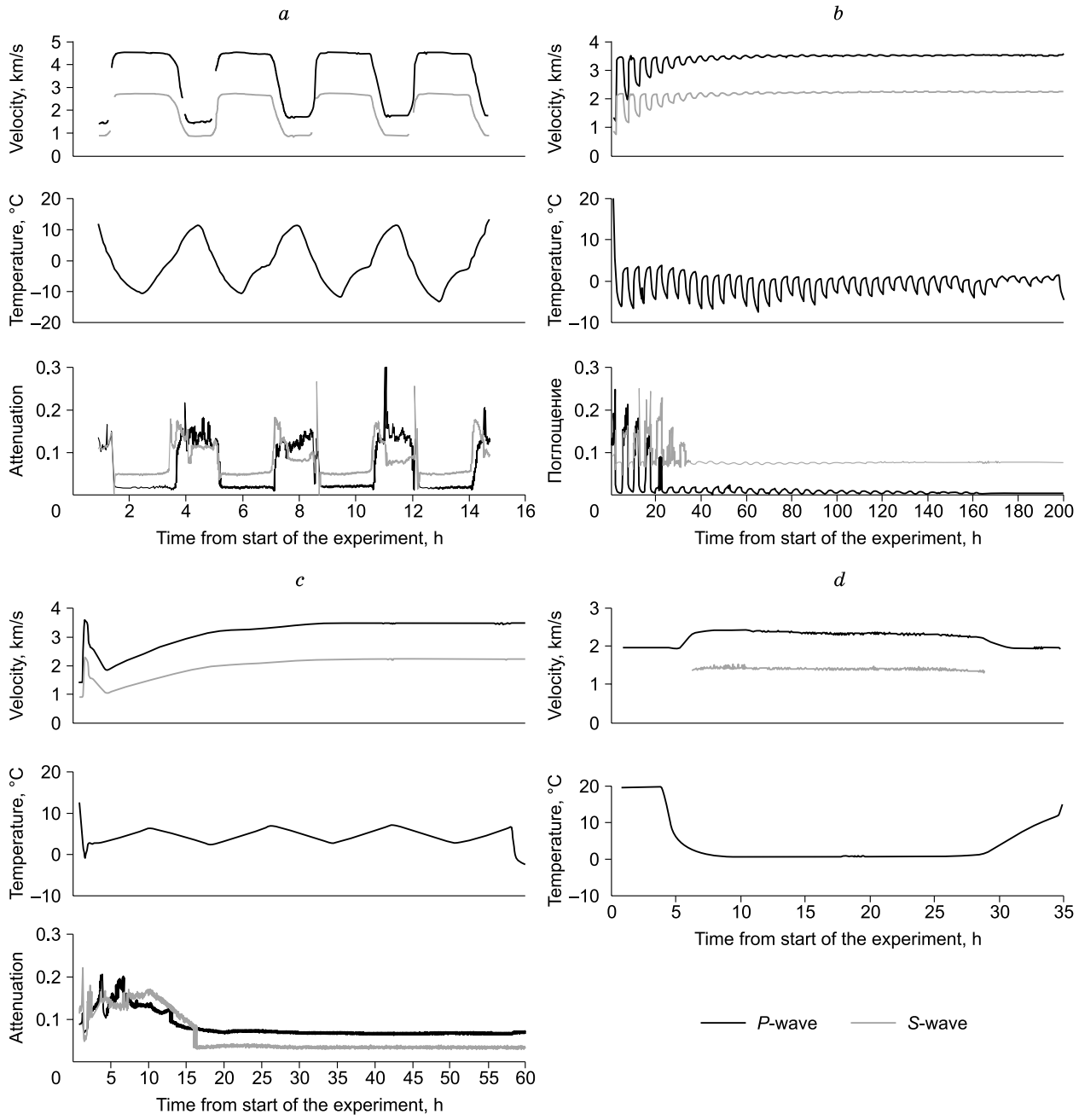

Fig. 2. Initial velocity, attenuation and temperature measurements in the samples containing water and ice (*a*); methane hydrate (*b*, *c*); and THF hydrate (*d*). *a*, Experiment (26.04.2016) with a sample containing water ($T > 0$) or ice ($T < 0$); the sample's initial porosity and water saturation: $K_p = 0.4$, $S_w = 0.92$. Its acoustic parameters after freezing: $v_P = 4520$ m/s, $v_S = 2720$ m/s, $Q_P^{-1} = Q_S^{-1} = 0.1–0.15$; *b*, experiment (14.06.2016) in a methane hydrate-bearing sample; the sample's initial water saturation and final hydrate saturation: $S_w = 0.32$ and $S_h = 0.4$. The sample's acoustic parameters after full hydrate formation: $v_P = 3500$ m/s, $v_S = 2240$ m/s; $Q_P^{-1} = 0.01$, $Q_S^{-1} = 0.8$; *c*, experiment (18.10.2016) with a methane hydrate-bearing sample; the sample's initial water saturation and final hydrate saturation: $S_w = 0.3$ and $S_h = 0.4$. The sample's acoustic parameters after full hydrate formation: $v_P = 3480$ m/s, $v_S = 2220$ m/s; $Q_P^{-1} = 0.03$, $Q_S^{-1} = 0.07$; *d*, experiment (06.09.2016) with a THF hydrate-bearing sample; the sample's initial THF concentration (C) in water solution and final hydrate saturation: $C = 10.66\%$, $S_h = 0.56$. The sample's acoustic parameters after full hydrate formation: $v_P = 2420$ m/s, $v_S = 1432$ m/s.

changes. While freezing they gradually grew to $v_P = 4520$ m/s and $v_S = 2730$ m/s during every cycle, and while defreezing they reduced to $v_P = 1650$ m/s and $v_S = 890$ m/s. A similar clear reaction to the phase transitions was demonstrated by the signal attenuation. In this experiment, the minimum inverse Q-factor values (0.02–0.05) were characteristic for frozen samples, and defreezing increased these values 3–5 times (up to 0.15).

Acoustic measurements in methane hydrate-bearing samples. In a subsequent series of experiments, the effect of methane hydrate concentration in samples on the velocities and attenuation of acoustic waves was investigated. Samples with different proportions of water and sand were placed in the setup chamber, which was then filled with methane at gas pressure of around 8–10 MPa to cleanse the system and remove air residuals. The temperature inside the chamber was also increased (generally up to ±7 °C) to obtain the conditions necessary for gas hydrate formation. For the indicated temperatures the applied pressure significantly exceeded the equilibrium one (at the pressure of 8 MPa, the hydrate decomposition temperature equals 11.3 °C), which remarkably increased hydrate formation. For the same reason, we changed the temperature in cycles leading to sequential freezing/defreezing of the samples. In this case, we relied on the notion that hydrate formation intensifies most at the boundary of the ice-water transition. The experiments in this series continued from 20 to 70 hours divided into 3–6 freezing/defreezing cycles. An experiment was stopped after complete hydrate formation due to full water transform to hydrate. In order to master the technique, we also performed a number of longer (150–240 h) experiments, each including from 30 to 40 freezing/defreezing cycles. The hydrate amount formed in a sample (S_h) was determined by its initial water concentration and can be estimated as:

$$S_h = (1.15 \cdot M_w \cdot \rho_s)/(\rho_h \cdot (V \cdot \rho_s - M_s)),$$

where M_s, denotes the sand mass, g; M_w, the initial water mass in a sample, g; V, the cell volume, cm^3; $\rho_s = 2.65$ g/cm^3, the sand density; $\rho_h = 0.914$ g/cm^3, the methane-hydrate density. Values M_s and M_w were determined while preparing the samples. The calculations showed that their hydrate volumetric content varied from 0.1 to 0.8 depending on the initial amount of water in a sample.

Figure 2*b*, *c* demonstrate the results of two such experiments performed in similar sand samples ($S_w \approx 0.3$–0.32), but in different times and under different conditions.

The first experiment lasted more than 200 hours being divided into more than 40 freezing/defreezing cycles with T changing from +2 to –3…–5 °C. Both the ice and methane hydrate were characterized by similarly fast acoustic wave velocities. These velocities ($v_P \approx 3400$–3500 m/s, $v_S \approx 2140$–2220 m/s) became steady at the initial stage of the experiment and maintained so due water-to-ice transition. While defreezing the ice was melting, reducing the velocities. At the same time hydrate was forming in the sample. Hydrate forming slowed the velocity reduction and, consequently, water loss in the pores. In 50–60 h, the velocities equalized at their maximum for all the temperatures, which meant all the available water transformed into hydrate. Once reached, this stage continued without changes for the next 150 h. Here it should be noted that a stabilized acoustic pattern while 0 °C crossing is a sign of complete hydrate formation, i.e., a sample no longer contains any water that can freeze.

The second experiment lasted about 60 hours at positive temperature (~2–7 °C). In this experiment hydrate formed without being interrupted by temporary freezing of the sample. Gradual hydrate forming in pores was traced from a constant increase of the acoustic velocities, which achieved their maximum values ($v_P = 3480$ m/s, $v_S = 2220$ m/s) in 30–40 hours when hydrate formation process completed.

Despite the significant differences in experimental conditions, a relatively similar amount of hydrates ($S_h \approx 0.4$) was obtained at relatively similar maximum values of acoustic wave velocities ($v_P \approx 3500$ m/s, $v_S \approx 2200$ m/s) reached at the final stage of the experiment. These results confirmed the consistency of laboratory setup operation and its ability to reproduce similar results in similarly prepared samples. On the other hand, the obtained results have demonstrated that at a low initial water saturation (about one-third of the pore space) sequential freezing/defreezing of a sample does not accelerate hydrate formation, which calls for more detailed experimental verification of the applied technique for different water saturation degrees.

The attenuation estimations performed based on the results of experimental investigation (Fig. 2*b*, *c*) demonstrated that the methane-hydrate saturated samples were characterized by a lower attenuation rate of about 0.03–0.07. In presence of unfrozen water, it increased up to about 0.15. A similar pattern was observed for the water/ice-saturated samples.

Acoustic measurements in THF hydrate-bearing samples. The objective of these experiments was studying the dependence of sample acoustic properties on the concentration of the hydrates formed from a water solution of a hydrate former (THF in particular). Preparing a sample, we mixed THF with distilled water until a necessary concentration was obtained and added in sand afterwards. The mixture was then put in a measuring cell placed in the setup chamber. All the operations were performed as quickly as possible due to THF high volatility. Hydrate formation started at atmospheric pressure after cooling the cell below 4 °C. The experiments lasted 25–50 hours in general, their temperature varying from RT to –5…–7 °C.

In the examined samples THF-solution concentration varied from 10 to 76 wt.%, so their hydrate saturation (S_h) changed with the range from 0.3 to 1. The S_h value was estimated from the following expression:

$$\text{for } C > C_0 \; S_h = \frac{1}{1 + \dfrac{C - C_0}{1 - C} \cdot 1.03},$$

$$\text{for } C < C_0 \; S_h = \frac{1}{1 + \left(\dfrac{C_0}{C} - 1 \right) \cdot 0.91},$$

where C, denotes the initial THF mass concentration in a solution, measured in mass percent while preparing the samples; $C_0 = 19.4$ wt.%, the stoichiometric THF concentra-

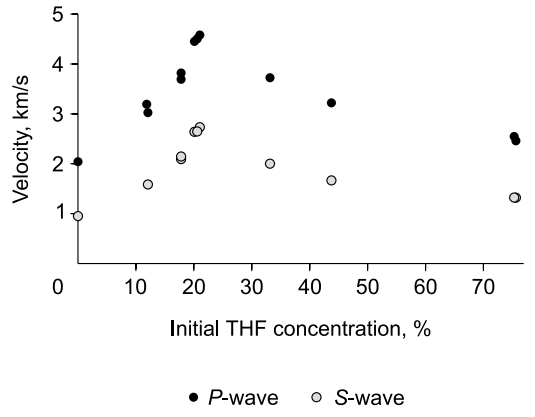

Fig. 3. v_P and v_S changes in THF hydrate-bearing samples depending on their initial THF concentration.

tion in a solution producing the maximum volumetric hydrate saturation (S_h = 1) in a sample with maximum measured acoustic wave velocities. The reliability of the expression above was confirmed by our experiments (Fig. 3) demonstrating that reducing (relative to C_0) THF concentration in a sample led to reduction of hydrate saturation, which manifested itself in a corresponding velocities change.

At $C < C_0$ the samples, apart from THF hydrate and sand, also contained water that got frozen after prominent temperature reduction, which, in a number of cases, significantly complicated interpretation of measurement results. At $C > C_0$ the samples could also contain (in addition to sand and THF hydrate) liquid THF. In such samples, no ice formed while freezing.

The experimental technique for THF hydrate-bearing samples had not been fully developed for the reasons indicated above that caused problems with proper signal registration (especially in case of *S*-waves). Figure 2*d* demonstrates the results of one of the most successful of such experiments. It lasted for 50 hours with the temperature varying from room temperature to ~1 °C. The increase in velocities marked the beginning of hydrate formation in the sample with a decrease in *T* to 4 °C (~21 h) Hydrate formation completed in about 25 hours after the experiment had started, and at about the same time the maximum values of acoustic velocities were registered: v_P = 2420 m/s (increased by 450 m/s) and v_S = 1430 m/s (increased by 180 m/s). The stable conditions for THF hydrates maintained in the sample an additional 20 h. Within this time period gradual velocity decrease was observed (v_P reduced more than by 100 m/s) that can be explained by on-going restructuring of the crystals in the hydrate body taking almost half of the pore space (Rydzy, 2014). Unfortunately, the experimental results did not permit to estimate the wave attenuation values.

ACOUSTIC PROPERTIES OF FROZEN AND HYDRATE-BEARING SAND SAMPLES

The series of performed experiments allowed us to obtain data on the acoustic properties of ice/hydrate-bearing sand samples. For further data processing, only the mean values of acoustic wave velocities and attenuations were used. The mean values were calculated from the measurements obtained after a sample's complete freezing or after hydrate formation was complete.

Acoustic wave velocities. To begin, let us consider the results for the ice/water-saturated samples. The experiments demonstrated that at the positive temperatures *P*- and *S*-waves did not depend on the amount of water in a sample (up to S_w = 0.95) and in average comprised: v_P = 1400 m/s and v_S = 900 m/s (varying within ±150 m/s). Such absence of relation between the parameters can be explained by that fact that at positive *T* and atmospheric pore pressure, acoustic waves propagates mainly through a sample's mineral matrix, i.e., even despite the sufficient amount of water in the pores, the sample behaves as if it is gas-saturated. It should be pointed out that a similar behavior was observed when studying water-saturated consolidated sandstones, in which *P*-wave velocity started to grow only at $S_w > 0.95$ (Nolet, 1990).

Water freezing in the pores led to an increase of both P- and S-wave velocities for the whole range of S_w variations (Fig. 4, *1*). The fastest growth was registered at the initial stage of ice filling the pores (up to about S_w = 0.4–0.5) and after that the growth rate decreased.

The observed dependence of *P*- and *S*-wave velocities on ice concentration is evidence of cementing model realization in the experiments. The ice has been binding the sand grains since the moment of its appearance in the pores and thus "cements" a sample, which leads to increased acoustic wave velocities. When freezing of the samples fully saturated with water is complete v_P increases to 4500 m/s, and v_S to 2700 m/s, i.e., the experiments with water-saturated samples have demonstrated that the acoustic wave velocities depend significantly on the initial water amount and the initial temperature of a sample.

Now, let us consider the results obtained for methane hydrate saturated samples. Figure 4, *2* shows the v_P and v_S es-

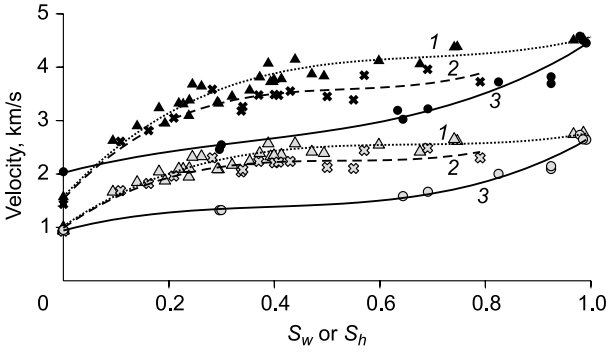

Fig. 4. Changes in the velocities of *P*- and *S*-waves in ice-saturated samples (*1*), methane hydrate-bearing samples (*2*) and THF hydrate-bearing samples (*3*) depending on either their water S_w (ice) or hydrate S_h saturation coefficient. The lines are the data after third degree polynomial approximation. Each point on the graph is a result of an independent long-term experiment.

timations for samples with different final values of volumetric gas hydrate content (S_h). It is apparent that even a small amount of methane hydrate provokes an abrupt increase of acoustic velocities (especially up to S_h = 0.3–0.4). With further growth of gas hydrate concentration, the velocities keep increasing but not that fast: at S_h = 0.8 they reach v_P = 3900 m/s, v_S = 2500 m/s. The obtained results demonstrate that the used technique of hydrate formation (injections of free methane in a water-saturated sample) makes the hydrate distribute in the pores following the cementing model as in the case of ice. Comparison of the ice and methane-hydrate graphs (Fig. 4, *1* and *2*) shows that for the S_h range in question, the hydrate-bearing samples are characterized by low acoustic wave velocities than those saturated with ice. This fact can be explained by different cementing types when filling the pores. In the case of ice, these are grains contacts that are cemented, which results in a significant velocities increase depending on the amount of the cementing material. The gas-hydrate, on the other hand, most likely follows the enveloping cementing pattern characterized by slower velocities growth (Dvorkin et al., 2000). There is another assumption (Rydzy, 2014) that the observed difference can be related to a gradual closing of the passes the gas penetrates into a sample by forming hydrate, which leads to slowed hydrate formation and velocity increase. To stimulate these processes, some researches included the mechanical procedures that broke hydrate walls in samples. For a number of reasons, our setup did not allow for such mechanical procedures.

Figure 4, *3* demonstrates the way the acoustic velocities depend on THF-hydrate volumetric content (S_h). For technical reasons we were not able to cover with samples the whole range of S_h values. However, the obtained data still enabled us to verify the character of acoustic wave velocity change depending on the amount of the THF hydrate forming from hydrate former water solution. First, we were able to register acoustic wave velocity increase for the whole range of S_h changes. At the initial stage (up to S_h = 0.6–0.7) the acoustic velocities grew slowly, while further increase of hydrate concentration (above S_h = 0.6–0.7) triggered their abrupt increase to $v_P \sim 4500$ and $V_s \sim 2600$ m/s, the values similar to those registered for complete ice saturation. These changes of acoustic velocities can be explained by that at the initial stage, the hydrate accumulates in the pores following the filling pattern and yet fails bind the sand grains. At this stage the velocities change insignificantly due to only partial replacement of the fluid by hydrates. Then THF hydrate starts cementing the grains (at $S_h > 0.6$–0.7), causing the abrupt growth in *P*- and *S*-wave velocities.

Acoustic wave attenuation. Modern high-frequency seismic tools enable one to estimate not only the velocities of the seismic waves propagating through sea bottom sediments but their attenuation as well (Lupinacci and Oliveira, 2015; Oliveira et al., 2017). These have been attempts to use these data for searching and studying of gas-hydrate deposits, as it was demonstrated that the attenuation of elastic oscillations was sensitive to presence of such accumulations in a formation (Priest et al., 2006). These attempts also stimulate interest in carrying out laboratory investigations into elastic wave attenuation in frozen and hydrate-bearing rocks. In this respect, in our study the obtained measurements were also used to estimate the attenuation based on the inverse Q-factor formula (1) for the samples with different values of water/ice, methane hydrate and THF saturation. Some of the results obtained have already been described in this paper, so this section we would like to compare the average attenuation values for the whole experimental series against the initial measurements of water/ice (S_w) and hydrate (S_h) content. The graphic visualization of this comparison is presented in Fig. 5, where the graphs demonstrate the linear trends.

Figure 5*a* shows how *P*- and *S*-wave attenuation in water/ice-saturated samples, depending on the initial S_w values. Despite the data spread, it can be seen that the elastic waves attenuate faster in water-saturated samples. In this case, the attenuation range comprises Q^{-1} = 0.09–0.16 (*P*-waves at-

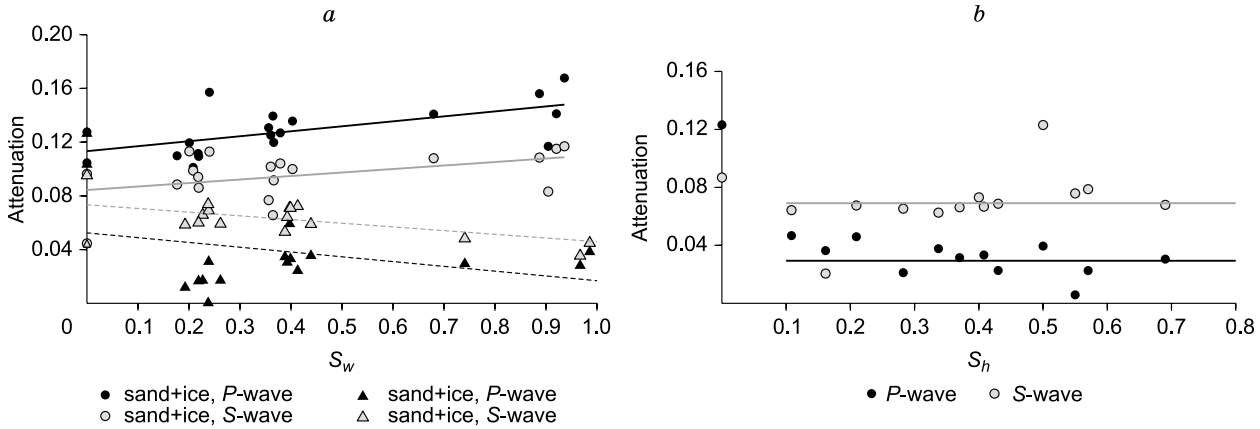

Fig. 5. Changes in the mean values attenuation (Q^{-1}) of *P*- and *S*-waves in water/ice- (*a*) and methane hydrate-bearing (*b*) samples depending on their S_w (ice) and S_h (hydrates). *a*, Water-saturated (round markers) and frozen (triangular markers) samples; *b*, methane hydrate-bearing samples.

tenuate faster), and the attenuation rate grows together with the growth of S_w. In the water-saturated samples the attenuation is determined by the volumetric fluid migration and sliping relative to the inclosing matrix triggered by elastic oscillations. Increase of S_w increases the fluid concentration and enhance the attenuation mechanisms.

For the frozen samples the pattern has been a reduced attenuation degree as in general (the attenuation range Q^{-1} = 0–0.07, *S*-waves attenuate faster) as in case of S_w increase. Here, the reduced attenuation can be explained by the cementing effect, so the higher S_w the more ice is formed in a sample. The ice increases the sample's cementation, which reduces the friction and sliping of sand granules and, consequently, decreases the attenuation rate.

Figure 5*b* presents estimation results for *P*- and *S*-wave attenuation values in methane hydrate-bearing samples in dependence on the initial S_h values. In absence of the hydrate (S_h = 0) the maximum attenuation was observed for both *P*- and *S*-waves ($Q^{-1} \approx$ 0.09–0.13). The initial S_h increase caused an abrupt attenuation increase, which then remained constant ($Q^{-1} \approx$ 0–0.08) for the whole range of S_h = 0.1–0.7. The average attenuation values comprised 0.03 for *P*-waves and 0.06 for *S*-waves. Changes in the attenuation correlated with the velocity data and confirmed our assumption about the cementing type of the hydrate body.

Estimations of acoustic wave attenuations in THF hydrate-bearing samples did not reveal any systematic dependence of Q^{-1} on S_h. The reason may have been the technical issues that occurred when carrying out experiments with these samples. In this respect, there has been no reason to interpret these data until they are either confirmed or disproved by an additional series of experiments.

The results obtained from this series of experiments in water/ice and methane hydrate-bearing samples require additional refinement and interpretation. Possibly, for obtaining more reliable information one has to improve the applied method of acoustic measurements, especially when it concerns THF hydrate-bearing samples.

DISCUSSIONS

At the initial stage of the study, the acoustic properties the samples containing different amounts of water and ice were investigated. It was established that the very first appearance of ice in a sample's pores triggered a fast growth of acoustic wave velocities, which is the evidence of ice cementing contacts between sand grains (Fig. 1*c*). The methane hydrate-bearing samples were formed using injections of free gas into the sand samples containing fresh water. This type of hydrate formation also resulted in the cementing pattern of pore filling (Fig. 1*d*), leading to slower growth of acoustic wave velocities caused by hydrate formation.

In the experiments with THF, hydrate formed from a water solution of a hydrating agent. At the initial stage (at $S_h <$ 0.6–0.7), the acoustic wave velocities changed insignificantly, which confirmed THF hydrates distributed in a sample following the pore-filling model (Fig. 1*a*). In this case the hydrate initially did not bind the sand grains, and binding only began at $S_h >$ 0.6–0.7.

The obtained velocity data allowed us to estimate the values of Poisson's ratios (υ) and YMs (E) for the studied samples. Without going into details, in this paper we only describe the general character of the changes of the average values of the said parameters. For all the sample types Poisson's ratio depends on the type of a matter filling the pores (water, ice, and hydrate) and has almost no dependence on the matter' concentration. The lowest mean value υ = 0.1 was obtained for the water-saturated samples. In the same samples after freezing υ grew almost two times up to 0.18, while in the hydrate-bearing samples this value was equal to 0.14. The maximum Poisson's ratio was registered in the samples containing THF hydrates. YM values remained constant (~ 2.75 GPa) for the whole range of water saturation at positive temperature. For the samples with ice and hydrates E grew together with the increase of hydrate and ice volumetric content: from 10–13 to 25–27 GPa (at S_w = 0.2–1 and S_h = 0.1–0.7).

Our results for the acoustic velocities are comparable to those published by foreign authors (Waite et al., 2004; Priest et al., 2005; Yun et al., 2005; Ebinuma et al., 2008; Lee et al., 2010; Ren et al., 2010; Rydzy, 2014; Schindler et al., 2017). Figure 6*a*, *b* bring together the dependencies of *P*- and *S*-wave velocities on methane-hydrate concentration in samples, obtained in different times.

The figure shows three types of v_P and v_S dependencies on S_h: a fast acceleration of the velocities at $S_h > 0$ followed by their deceleration (that is where our data come to); a slow growth followed by acceleration; and a slow linear growth of the velocities. The observed regularities are most likely determined by distribution of the hydrate forming in the pores. Probably in the first and third cases we observed cementing hydrate, while in the second—the filling hydrate replaced by cementing one. The differences of the results obtained can also be determined by the differences in laboratory-setup designs and sample preparation methods.

Figure 6*c* compares the results by foreign authors with our results obtained for THF hydrate-bearing samples. The comparison was complicated by the significant differences in absolute values that occurred due to the different matrix compositions used in the experiments. To compensate these differences the graphs describing v_P and v_S dependences on S_h graphs were displaced in a way to match the initial velocities (at S_h = 0). The compared data have shown that THF hydrates at the initial stage (up to S_h = 0.3–0.4) form pore-filling hydrates, which at higher hydrate saturation start cementing a sample.

The performed analysis has demonstrated that our results are in good correlation with the results obtained by our foreign colleagues that were obtained in about similar conditions.

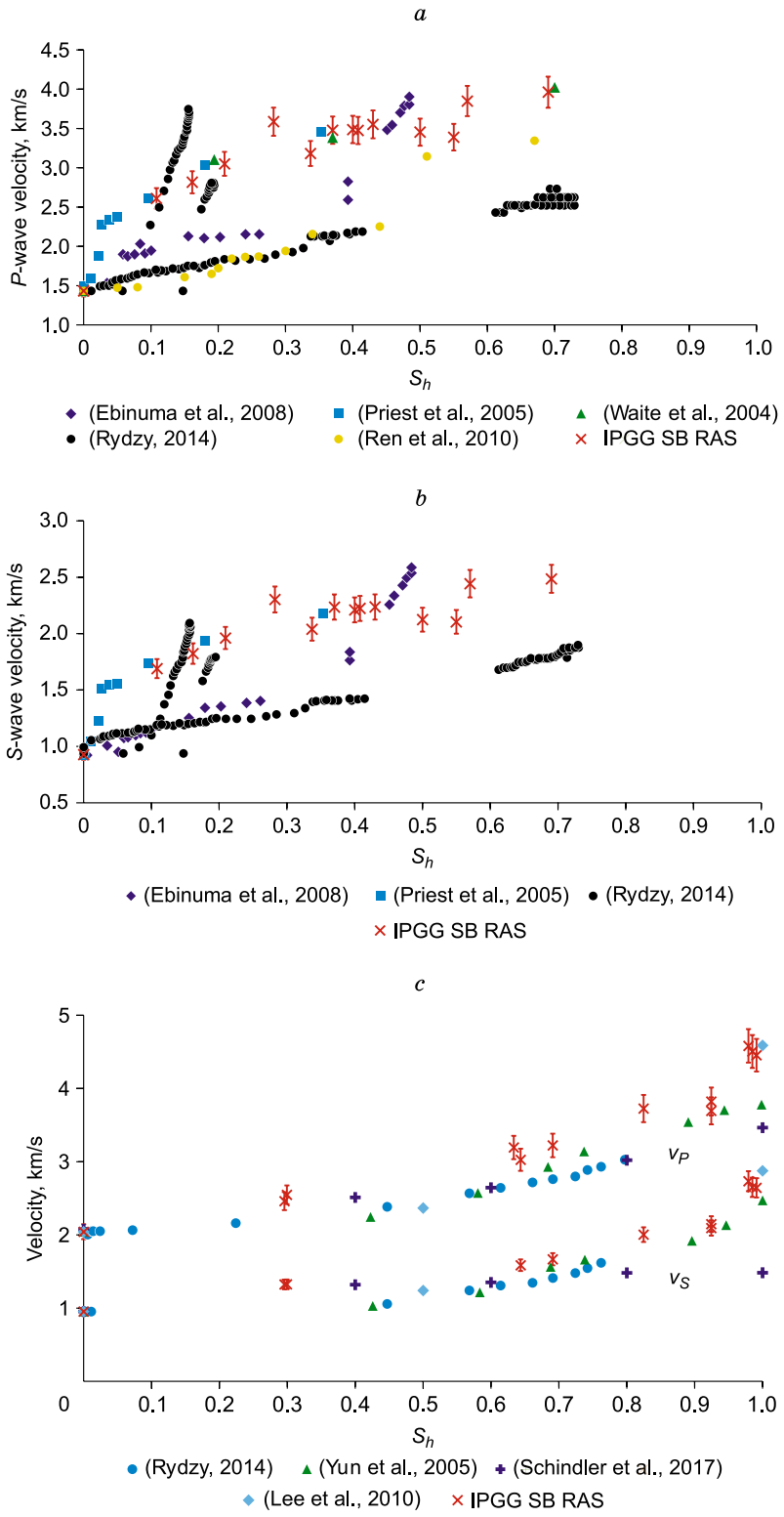

Fig. 6. Comparative analysis of our results (IPGG SB RAS) of measuring acoustic wave velocities in sand samples bearing methane hydrate (*a*, *b*) and THF hydrate (*c*) saturated sand samples against those obtained by foreign authors (Waite et al., 2004; Priest et al., 2005; Yun et al., 2005; Ren et al., 2010; Ebinuma et al., 2008; Lee et al., 2010; Rydzy, 2014; Schindler et al., 2017). For our data, the dashes mark the boundaries of a relative 5% error.

CONCLUSIONS

In the course of our study, we have designed and put in operation a laboratory setup that (first time in Russia) allows to perform complex experiments into modeling of hydrate-bearing samples and measuring their acoustic properties. The setup relative measurement accuracy comprises 1% for consolidated and 5–6% for nonconsolidated samples. Using the setup more than 100 experiments with the sand samples containing different volumes of water, ice, methane hydrate and THF, have been performed. The experiments have confirmed the setup stability while working in autonomous mode and demonstrated a necessary level of repeatability. The obtained dependencies of acoustic velocities have been interpreted as the models corresponding to different types of pore-filling with either ice or hydrate: cementing the contacts between sand grains while ice formation; enveloping cementing while methane hydrate formation; and pore-filling while THF-hydrate formation. The dependencies can be used for interpretation of seismic data from areas embracing hydrate deposits and permafrost. However, it is necessary to point out that the considered results have been obtained for ideal conditions such as quartz sand, distilled water, etc. Real incompetent rocks (sand beds, loams, cryolithozones, argillaceous marine sediments, coals, etc.) are more complex structures, and for accurate characterization of their acoustic properties one has to continue experiments in the samples, whose structure is similar to the one of natural rock.

The study has been a part of the planned research agenda of Geophysics Department of A.A. Trofimuk Institute of Petroleum Geology and Geophysics, SB RAS, and carried out with funding from the Russian Science Foundation (grant No. 14-17-00511). The authors would like to thank N.A. Golikov, A.Yu. Manakov, and M.E. Permyakov for their assistance in the performing the experiments.

REFERENCES

Akselrod, S.M., 2009. Prospecting and pilot operation of gas hydrate deposits (based on foreign publications). Karotazhnik 8 (185), 92–123.

Chuvilin E.M., Gyryeva, O.M., 2009. Experimental investigation of CO_2 gas hydrate formation in porous media of frozen and freezing sediments. Kriosfera Zemli 13 (3), 70–79.

Duchkov, A.D., Golikov, N.A., Duchkov, A.A., Manakov, A.Yu., Permyakov, M.E., Drobchik, A.N., 2015. Laboratory equipment to study the acoustic properties of hydrate-bearing rocks seismic tools. Seismicheskie Pribory 51 (2), 44–55.

Duchkov, A.D., Duchkov, A.A., Manakov, A.Yu., Permyakov, M.E., Golikov, H.A., Drobchik, A.N., 2017a. Laboratory modeling and measurement of the acoustic properties of methane-bearing rock samples. Dokl. Earth Sci. 472 (1), 44–48.

Duchkov, A.D., Duchkov, A.A., Permyakov, M.E., Manakov, A.Yu., Drobchik, A.N., Golikov, N.A., 2017b. Acoustic properties of hydrate-bearing sand samples:laboratory measurements (setup, methods, and results). Russian Geology and Geophysics (Geologiya i Geofizika) 58 (6), 727–737 (900–914).

Duchkov, A.D., Duchkov, A.A., Dugarov, G.A., Drobchik, A.N., 2018. Velocities of ultrasonic waves in sand samples containing water, ice, or methane and tetrahydrofuran hydrates (laboratory measurements). Dokl. Earth Sci 478 (1), 74–78.

Dugarov, G.A., Duchkov, A.A., Duchkov, A.D., Drobchik, A.N., 2017. Laboratory studies of the acoustic properties of hydrate-bearing sediments. Uchenye Zapiski Fizicheskogo Facul'teta Mosk. Univ., No. 5, 1750812.

Dvorkin, J., Nur, A., 1996. Elasticity of high-porosity sandstones: Theory for two North Sea sets. Geophysics 61, 1363–1370.

Dvorkin, J., Prasad, M., Sakai, A., Lavoie, D., 1999. Elasticity of marine sediments: Rock physics modeling. Geophys. Res. Lett. 26 (12), 1781–1784.

Dvorkin, J., Helgerud, M.B., Waite, W.F., Kirby, S.H., Nur, A., 2000. Introduction to physical properties and elasticity models (Ch. 20), in: Max, M.D. (Ed.), Natural Gas Hydrate in Oceanic and Permafrost Environments. Kluwer Academic Publishers, Dordrecht, pp. 245–260.

Ebinuma, T., Suzuki, K., Oyama, H., Narita, H., 2008. Ultrasonic wave velocities associated with formation and dissociation of methane hydrate in artificial sandy sediment, in: Presented at the 2008 Offshore Technology Conference, Paper OTC 19260, Houston, TX, May, pp. 5–8.

Ecker, C., Dvorkin, J., Nur, A., 1998. Sediments with gas hydrates: internal structures from seismic AVO. Geophysics 63, 1659–1669.

Gabitto, J.F., Tsouris, C., 2010. Physical properties of gas hydrates: A review. J. Thermodyn. ID 271291, DOI: 10.1155/2010/271291.

Ginsburg, G.D., Soloviev, V.A., 1994. Submarine Gas Hydrates [in Russian]. VNIIOkeanologiya, St.-Petersburg.

GOST 21153.7-75, 1975. Earth Materials. *P*- and *S*-Wave Velocity Detection Method [in Russian]. Izd. Setupartov, Moscow.

Hu, G.W., Ye, Yu.G., Zhang, J., Liu, C.L., Diao, S.B., Wang, J.S., 2010. Acoustic properties of gas hydrate-bearing consolidated sediments and experimental testing of elastic velocity models. J. Geophys. Res. Solid Earth 115, B02102.

Istomin, V.A., Yakushev, V.S., 1992. Gas Hydrates in Nature [in Russian]. Nedra, Moscow.

Khlystov, O.M., 2006. New findings of gas hydrates in the Baikal bottom sediments. Russian Geology and Geophysics (Geologiya i Geofizika) 47 (8), (979–981).

Knunyants, I.L. (Ed.), 1983. Chemical Encyclopedia [in Russian]. Sovetskaya Entsiklopediya, Moscow.

Lee, J.Y., Yun, T.S., Santamarina, J.C., Ruppel, C., 2007. Observations related to tetrahydrofuran and methane hydrates for laboratory studies of hydrate-bearing sediments. Geochem. Geophys. Geosyst. 8, Q06003.

Lee, J.Y., Francisca, F.M., Santamarina, J.C., Ruppel, C., 2010. Parametric study of the physical properties of hydrate-bearing sand, silt, and clay sediments: 2. Small-strain mechanical properties. J. Geophys. Res. 115, B11105.

Lee, M.W., Hutchinson, D.R., Collett, T.S., Dillon, W.P., 1996. Seismic velocities for hydrate-bearing sediments using weighted equation. J. Geophys. Res. 101, 20,347–20,358.

Li, D., Wang, D., Liang, D., 2011. *P*-wave of hydrate-bearing sand under temperature cycling. Geophysics 76 (1), E1–E7.

Lupinacci, W.M., Oliveira, S.A.M., 2015. Q-factor estimation from the amplitude spectrum of the time–frequency transform of stacked reflection seismic data. J. Appl. Geophys. 114, 202–209.

Makogon, Y.F., Holditch, S.A., Makogon, T.Y., 2007. Natural gas-hydrates—A potential energy source for the 21st century. J. Pet. Sci. Eng. 56 (1), 14–31.

Manakov, A.Yu., Duchkov, A.D., 2017. Laboratory modeling of hydrate formation in rock specimens (a review). Russian Geology and Geophysics (Geologiya i Geofizika) 58 (2), 240–252 (290–307).

Mazurenko, L.L., Soloviev, V.A., 2003. Worldwide distribution of deep-water fluid venting and potential occurrences of gas hydrate accumulations. Geo-Mar. Lett. 23 (304), 162–176.

Measurement and Interpretation of Seismic Velocities and Attenuation in Hydrate-Bearing Sediments, 2017. Colorado School of Mines

and United States Geological Survey, Project 2012–2016 (https://www.netl.doe.gov/research/oil-and-gas/project-summaries/methane-hydrate/de-fe0009963).

Nolet, G. (Ed.), 1990. Seismic Tomography [in Russian]. Mir, Moscow.

Obzhirov, A.I., Korovitskaya, E.V., Pestrikova, N.L., Telegin, Yu.A., 2012. Hydrocarbon saturation oil-gas deposit and gas hydrates in the Okhotsk Sea. Podvodnye Issledovaniya i Robototekhnika 14 (2), 55–62.

Oliveira, F.S., de Figueiredo, J.J.S., Oliveira, A.G., Schleicher, J., Araújo, I.C.S., 2017. Estimation of quality factor based on peak frequency-shift method and redatuming operator: Application in real data set. Geophysics 82 (1), N1–N12.

Priest, J.A., Best, A.I., Clayton, C.R.I., 2005. A laboratory investigation into seismic velocities of methane gas hydrate-bearing sand. J. Geophys. Res. 110, B04102.

Priest, J., Best, A.I., Clayton, C.R.I., 2006. Attenuation of seismic waves in methane gas hydrate-bearing sand. Geophys. J. Int. 164, 149–159.

Ren, S.R., Liu, Y., Liu, Y., Zhang, W., 2010. Acoustic velocity and electrical resistance of hydrate bearing sediments. J. Pet. Sci. Eng. 70, 52–56.

Riedel, M., Willoughby, E.C., Chopra, S. (Eds.), 2010. Geophysical Characterization of Gas Hydrates. SEG Geophysical Developments Series, Vol. 14. Society of Exploration geophysicists, Tulsa.

Rydzy, M.B., 2014. The Effect of Hydrate Formation on the Elastic Properties of Unconsolidated Sediment. DrSci. Thesis (https://dspace.library.colostate.edu/bitstream/handle/11124/356/Rydzy_mines_0052E_10396.pdf).

Schindler, M., Batzle, M.L., Prasad, M., 2017. Micro X-Ray computed tomography imaging and ultrasonic velocity measurements in tetrahydrofuran-hydrate-bearing sediments. Geophys. Prosp. 65, 1025–1036.

Sloan, E.D., 2003. Fundamental principles and applications of natural gas hydrates. Nature 426 (6964), 353–363.

Tonn, R., 1991. The determination of the seismic quality factor Q from VSP data: A comparison of different computational methods. Geophysics 39, 1–27

Waite, W.F., Winters, W.J., Mason D.H., 2004. Methane hydrate in partially water-saturated sand. Am. Mineral. 89, 1202–1207.

Waite, W.F., Santamarina, J.C., Cortes, D.D., Dugan, B., Espinoza, D.N., Germaine, J., Jang, J., Jung, J.W., Kneafsey, T.J., Shin, H., Soga, K., Winter, W.J., Yun, T.-S., 2009. Physical properties of hydrate-bearing sediments. Rev. Geophys. 47, RG4003, 1–38.

Yakushev, V.S., 2009. Natural Gas and Gas Hydrates in Cryolithozone [in Russian]. VNIIGAS, Moscow.

Ye, Yu., Liu, Ch. (Eds.), 2013. Natural Gas Hydrates. Experimental Techniques and Their Applications. Springer-Verlag, Berlin–Heidelberg.

Yun, T.S., Francisca, F.M., Santamarina, J.C., Ruppel, C., 2005. Compressional and shear wave velocity in uncemented sediment containing gas hydrate. Geoph. Res. Lett. 32, L10609.

Editorial responsibility: M.I. Epov